Acute Posttraumatic Symptoms Are Associated With Multimodal Neuroimaging Structural Covariance Patterns: A Possible Role for the Neural Substrates of Visual Processing in Posttraumatic Stress Disorder

Supplemental Information

Supplementary Methods

Diffusion Tensor Imaging

Diffusion tensor imaging (DTI) of the white matter skeleton was completed to derive metrics of white matter microstructure. The processing pipeline was developed according to the recommendations of the ENIGMA consortium (http://enigma.ini.usc.edu/protocols/dti-protocols/). First, non-weighted volumes (i.e., b0 volumes) were motion corrected and averaged to serve as a reference for further processing. Motion and eddy current effects in the diffusion weighted imaging (DWI) data were reduced using the 'eddy' subroutine in the FMRIB Software Library (FSL) (1,2) to register the diffusion weighted volumes to the averaged non-weighted volume (1,3). Susceptibility effects were corrected using nonlinear warping of the DWI data to the participant's T1-weighted anatomical scan (4). T1-weighted images were skull-stripped using the Robust Brain Extraction (ROBEX) tool (5), followed by bias-correction using the FSL FAST routine (6), and were then contrast inverted to match the averaged non-weighted volume. Nonlinear warping was completed through the Symmetric Normalization (SyN) routine in the Advanced Normalization Tools (ANTs) suite (7). SyN was first used to warp the averaged non-weighted volume to the anatomical image, and the resulting warp parameters were applied to the full DWI data. DWI data were then down-sampled to a 2mm isotropic grid-spacing and fit with a tensor model (FMRIB Diffusion Toolbox). Tract-Based Spatial Statistics (TBSS) processing was implemented following the ENIGMA-DTI working group processing standards to generate FA

skeletal maps (8,9). First, FA maps were non-linearly registered to the standard ENIGMA FA map in Montreal Neurological Institute (MNI) standard space (9). The ENIGMA FA skeleton map was then projected onto each subject's FA maps in standard space. Visual inspection to ensure both correct tensor fitting and skeleton projection was completed as suggested by the ENIGMA-DTI working group (http://enigma.ini.usc.edu/protocols/dti-protocols/). This process was repeated to obtain maps of mean diffusivity (MD) and mode of the diffusion tensor (MO).

Voxel Based Morphometry

Voxel-based morphometry (VBM) was completed using standard FSL routines (i.e., FSLVBM) (1,10,11). T1-weighted MRI data were skull-stripped and segmented into grey matter maps in native space, then warped to MNI 152 standard space using non-linear registration (12). A grey matter template for the present study was then generated from an average of the standard space images that were subsequently flipped along the x-axis to create a left-right symmetric volume. Next, grey matter segmented images in native space were non-linearly registered to the study template and modulated by the Jacobian determinant to adjust for local expansion (or contraction) due to the non-linear component of the spatial transformation. These normalized maps were then concatenated, smoothed using a 4 mm full-width at half-maximum (FWHM) Gaussian Kernel, and re-masked by a participant-derived gray matter mask to index brain gray matter volume (GMV). All data were visually inspected prior to and after FSLVBM processing. Two participants were excluded from the analyses based on poor data quality that did not allow for accurate segmentation of GMV.

Cortical Reconstruction

Cortical surface maps were reconstructed through FreeSurfer within the FMRIPREP framework (13,14). The T1-weighted images were bias-field corrected (15) and skull-stripped via ANTs. Cortical surfaces were reconstructed using recon-all in FreeSurfer (16), and the brain mask estimated previously was refined with a custom variation of the method to reconcile ANTs-derived and FreeSurfer-derived segmentations of the cortical gray-matter of Mindboggle (17). Individual participant maps of cortical thickness (CT) and pial surface area (PSA) were resampled into the fsaverage space and smoothed at a range of 10 mm FWHM. As discussed in the VBM processing section, two participants data were corrupted which prevented successful segmentation and these participants were excluded.

Supplementary Results

Associations between acute posttraumatic stress and structural covariance profile three

Although it did not survive multiple comparison correction, we observed a curvilinear relationship between structural covariance profile (SCP)-3 and 1-month mPSS scores. SCP-3 reflected a positive association with structural covariance networks (SCNs) SCN-4 and SCN-28, but a negative association with SCN-27. Collectively, this profile represented reduced mean diffusivity (MD) along the white matter skeleton, particularly in the body of the fornix, and reduced gray matter volume (GMV) and pial surface area (PSA) of the anterior cingulate cortex and superior temporal gyrus (STG)/temporoparietal junction (TPJ) (Figures S1 and S3). Follow-up regressions revealed no significant curvilinear relationship between SCP-3 and re-experiencing [$t(66) = 1.88$, $p = 0.064$, $\beta = 0.26$], avoidance [$t(66) = 1.81$, $p = 0.075$, $\beta = 0.33$] or arousal [$t(66) = 1.04$, $p = 0.303$, $\beta = 0.18$] scores. Further, SCP-3 did not vary linearly or curvilinearly with BDI-

II [t(66) = 0.24, p = 0.812, β = 0.03] scores. SCP-3 was not predictive of changes in mPSS scores from 1 to 12 months.

Exploratory follow-up regressions of structural covariance network associations with acute posttraumatic stress

Primary analyses revealed a curvilinear association between 1-month mPSS scores and two structural covariance profiles (SCP), specifically, SCP-3 and SCP-8. We thus completed follow-up regression analyses to identify which structural covariance networks (SCNs) that contributed to the SCP may show the strongest associations with 1-month mPSS scores. For SCP-3, we found that 1-month mPSS scores were significantly and curvilinearly associated with loadings on SCN-27 [t(66) = -2.72, p =0.008, β = -0.37], but not SCN-4 [t(66) = 1.61, p = 0.112, β = 0.22] or SCN-28 [t(66) = -1.14, p = 0.257, β = -0.17]. For SCP-8, we found that 1-month mPSS scores were significantly and curvilinearly associated with SCN-16 [t(66) = 3.17, p = 0.002, β = 0.44], but not SCN-18 [t(66) = -0.05, p = 0.957, β = -0.00] or SCN-22 [t(66) = 1.02, p =0.310, β = 0.14].

Supplementary Discussion

We identified a structural covariance profile (SCP-3) that reflected reduced mean diffusivity (MD) within the white matter skeleton, particularly the body of the fornix, as well as reduced gray matter volume (GMV) and pial surface area (PSA) within the anterior cingulate cortex (ACC), superior temporal gyrus (STG), and temoroparietal junction (TPJ). The SCP was positively and curvilinearly associated with mPSS scores at 1 month. Although not significant, we observed a trend-level relationship between loadings on this SCP and re-experiencing sub-scale scores. Thus, lower gray matter density in the ACC, STG, and TPJ, but greater white matter integrity within the fornix, inferior longitudinal fasciculus (ILF), and inferior fronto-occipital

fasciculus (IFOF), appear to be related to greater acute posttraumatic stress - and potentially re-experiencing - severity. We note however that the patterns of MD reduction, particularly in SCN-4, were somewhat diffuse across the white matter skeleton and may instead be related to white matter integrity more broadly. Reduced ACC and STG gray matter is consistent with prior reports in chronic PTSD (18–23) although STG findings are somewhat mixed (24,25). The greater integrity of the fornix in this SCP is notable as the fornix is a key white matter tract interconnecting the hippocampus with other subcortical structures such as the hypothalamus and nucleus accumbens, and may further be related to white matter projections to the PFC (26). The ACC and hippocampus are known to play a role in fear memory processes (27), and the fornix may also facilitate fear and declarative memory processes (26), and by extension, memories of the traumatic event. We have previously observed that dysconnectivity between the ACC and hippocampus in PTSD patients is related to disrupted fear inhibition (28). Further, the TPJ is also thought to support memory retrieval processes (29). Thus, one possible interpretation of the SCP and acute posttraumatic severity is that greater loadings reflect greater facilitation of fearful memories, such as those that are related to the trauma, that are not adequately regulated or inhibited.

Supplementary References

1. Smith SM, Jenkinson M, Woolrich MW, Beckmann CF, Behrens TEJ, Johansen-Berg H, *et al.* (2004): Advances in functional and structural MR image analysis and implementation as FSL. *NeuroImage*, vol. 23 23. https://doi.org/10.1016/j.neuroimage.2004.07.051

2. Jenkinson M, Beckmann CF, Behrens TEJ, Woolrich MW, Smith SM (2012): Review FSL. *Neuroimage* 62: 782–790.

3. Andersson JLR, Sotiropoulos SN (2016): An integrated approach to correction for off-resonance effects and subject movement in diffusion MR imaging. *Neuroimage* 125: 1063–1078.

4. Wang S, Peterson DJ, Gatenby JC, Li W, Grabowski TJ, Madhyastha TM (2017): Evaluation of field map and nonlinear registration methods for correction of susceptibility artifacts in diffusion MRI. *Front Neuroinform* 11. https://doi.org/10.3389/fninf.2017.00017

5. Iglesias JE, Liu CY, Thompson PM, Tu Z (2011): Robust brain extraction across datasets and comparison with publicly available methods. *IEEE Trans Med Imaging* 30: 1617–1634.

6. Zhang Y, Brady M, Smith S (2001): Segmentation of brain MR images through a hidden Markov random field model and the expectation-maximization algorithm. *IEEE Trans Med Imaging* 20: 45–57.

7. Avants B, Tustison N, Song G (2009): Advanced Normalization Tools (ANTS). *Insight J* 1–35.

8. Smith SM, Jenkinson M, Johansen-Berg H, Rueckert D, Nichols TE, Mackay CE, *et al.* (2006): Tract-based spatial statistics: Voxelwise analysis of multi-subject diffusion data. *Neuroimage* 31: 1487–1505.

9. Jahanshad N, Kochunov P V., Sprooten E, Mandl RC, Nichols TE, Almasy L, *et al.* (2013): Multi-site genetic analysis of diffusion images and voxelwise heritability analysis: A pilot project of the ENIGMA-DTI working group. *Neuroimage* 81: 455–469.

10. Douaud G, Smith S, Jenkinson M, Behrens T, Johansen-Berg H, Vickers J, *et al.* (2007): Anatomically related grey and white matter abnormalities in adolescent-onset schizophrenia. *Brain* 130: 2375–2386.

11. Good CD, Johnsrude IS, Ashburner J, Henson RNA, Friston KJ, Frackowiak RSJ (2001): A voxel-based morphometric study of ageing in 465 normal adult human brains. *Neuroimage* 14: 21–36.

12. Andersson JLR, Jenkinson M, Smith S (2007): Non-linear registration aka spatial normalisation. *FMRIB Technical Report TRO7JA2*. Retrieved from http://fmrib.medsci.ox.ac.uk/analysis/techrep/tr07ja2/tr07ja2.pdf

13. Esteban O, Markiewicz CJ, Blair RW, Moodie CA, Isik AI, Erramuzpe A, *et al.* (2019): fMRIPrep: a robust preprocessing pipeline for functional MRI. *Nat Methods* 16: 111–116.

14. Gorgolewski K, Burns CD, Madison C, Clark D, Halchenko YO, Waskom ML, Ghosh SS (2011): Nipype: A flexible, lightweight and extensible neuroimaging data processing framework in Python. *Front Neuroinform* 5. https://doi.org/10.3389/fninf.2011.00013

15. Tustison NJ, Avants BB, Cook PA, Zheng Y, Egan A, Yushkevich PA, Gee JC (2010): N4ITK: Improved N3 bias correction. *IEEE Trans Med Imaging* 29: 1310–1320.

16. Dale AM, Fischl B, Sereno MI (1999): Cortical surface-based analysis: I. Segmentation and surface reconstruction. *Neuroimage* 9: 179–194.

17. Klein A, Ghosh SS, Bao FS, Giard J, Häme Y, Stavsky E, *et al.* (2017): Mindboggling morphometry of human brains. *PLoS Comput Biol* 13. https://doi.org/10.1371/journal.pcbi.1005350

18. Woodward SH, Schaer M, Kaloupek DG, Cediel L, Eliez S (2009): Smaller global and regional cortical volume in combat-related posttraumatic stress disorder. *Arch Gen Psychiatry* 66: 1373–1382.

19. Hunter M, Villarreal G, McHaffie GR, Jimenez B, Smith AK, Calais LA, *et al.* (2011): Lateralized abnormalities in auditory M50 sensory gating and cortical thickness of the superior temporal gyrus in post-traumatic stress disorder: Preliminary results. *Psychiatry Res - Neuroimaging* 191: 138–144.

20. Rauch SL, Shin LM, Segal E, Pitman RK, Carson MA, McMullin K, *et al.* (2003): Selectively reduced regional cortical volumes in post-traumatic stress disorder. *Neuroreport* 14: 913–916.

21. Woodward SH, Kaloupek DG, Streeter CC, Martinez C, Schaer M, Eliez S (2006): Decreased anterior cingulate volume in combat-related PTSD. *Biol Psychiatry* 59: 582–587.

22. Bing X, Qiu MG, Ye Z, Zhang JN, Min L, Han C, *et al.* (2013): Alterations in the cortical thickness and the amplitude of low-frequency fluctuation in patients with post-traumatic stress disorder. *Brain Res* 1490: 225–232.

23. Rogers MA, Yamasue H, Abe O, Yamada H, Ohtani T, Iwanami A, *et al.* (2009): Smaller amygdala volume and reduced anterior cingulate gray matter density associated with history of post-traumatic stress disorder. *Psychiatry Res - Neuroimaging* 174: 210–216.

24. De Bellis MD, Keshavan MS, Frustaci K, Shifflett H, Iyengar S, Beers SR, Hall J (2002): Superior temporal gyrus volumes in maltreated children and adolescents with PTSD. *Biol Psychiatry* 51: 544–552.

25. De Bellis MD, Keshavan MS, Shifflett H, Iyengar S, Dahl RE, Axelson DA, *et al.* (2002): Superior temporal gyrus volumes in pediatric generalized anxiety disorder. *Biol Psychiatry* 51: 553–562.

26. Jang SH, Kwon HG (2014): Perspectives on the neural connectivity of the fornix in the human brain. *Neural Regen Res* 9: 1434–1436.

27. Knight DC, Cheng DT, Smith CN, Stein EA, Helmstetter FJ (2004): Neural Substrates Mediating Human Delay and Trace Fear Conditioning. *J Neurosci* 24: 218–228.

28. Fani N, King TZ, Brewster R, Srivastava A, Stevens JS, Glover EM, *et al.* (2015): Fear-potentiated startle during extinction is associated with white matter microstructure and functional connectivity. *Cortex* 64: 249–259.

29. Igelström KM, Webb TW, Kelly YT, Graziano MSA (2016): Topographical organization of attentional, social, and memory processes in the human temporoparietal cortex. *eNeuro* 3: 1363–1377.

Table S1. Medication and co-morbid diagnoses of sample

General usage	Medications	# of participants
Antidepressant	Trazadone, Zoloft, Elavil, Cymbalta, Citalopram	5
ACE Inhibitors	Lisinopril	2
Diabetes	Detemir, Metformin, Lantis, Novolog	3
Beta blocker	Atenolol	1
Bipolar disorder	Depakote	1
Calcium channel blocker	Amlodipine	3
NSAID Pain reliever	Naproxen	1
Opioids	Tramodol, Percocet, Oxycodone	3
Birth control	Depovera, Mirena	2
Narcotics	Methadone	1
Other pain medications	Cyclobenzapine, Gabapentin, Topamax	3
Other blood pressure medicine	Hydrochlorothiazide	1

Co-morbid diagnoses	# of participants
Depression	15
Hypomania	3
Mania	5
Alcohol use	
Dependence	6
Abuse	6
Substance use	
Dependence	3
Abuse	2
Psychotic disorders	
Current	1
Lifetime	1

Table S2. T1 and diffusion weighted imaging acquisitions.

	Scanner 1 (n = 22)	***Scanner 2 (n = 10)***	***Scanner 3 (n = 46)***
T1-weighted imaging	**MPRAGE**: **TR** = 2300ms, **TE** = 2.72ms, **TI** = 900ms, **flip angle** = 9, **FOV** = 256mm, **slices** = 160, **Voxel size** = 1.3mm x 1.3mm x 1.2mm, 0.6mm gap	**MPRAGE**: **TR** = 2300ms, **TE** = 2.72ms, **TI** = 900ms, **flip angle** = 9, **FOV** = 256mm, **slices** = 160, **Voxel size** = 1.3mm x 1.3mm x 1.2mm, 0.6mm gap	**MEMPRAGE**: **TR** = 2530ms, **TEs** = 1.74/3.6/5.46/7.32ms, **TI** = 1260ms, **flip angle** = 7, **FOV** = 256mm, **slices** = 176, **Voxel size** = 1mm x 1mm x 1mm, 0.5mm gap
Diffusion weighted imaging	**TR** = 3493ms, **TE** = 108.4ms, **FOV** = 212mm, **voxel size** = 2mm x 2mm x 2mm, **b-value** = 1000 s/mm2, sixty directions, 4 b0 images	**TR** = 3493ms, **TE** = 108.4ms, **FOV** = 212mm, **voxel size** = 2mm x 2mm x 2mm**, b-value** = 1000 s/mm2, sixty directions, 4 b0 images	**TR** = 7700ms, **TE** = 85ms, **FOV** = 212mm, **voxel size** = 2mm x 2mm x 2mm, **b-value** = 1000 s/mm2, sixty-four directions, 7 b0 images

Table S3. Structural covariance network loadings for each structural covariance profile.

	SCP-1	SCP-2	SCP-3	SCP-4	SCP-5	SCP-6	SCP-7	SCP-8
SCN-0	**-0.947**	-0.114	0.02	-0.014	0.085	0.054	0.052	0.033
SCN-2	-0.027	**0.803**	-0.082	-0.004	0.1	0.087	0.072	0.016
SCN-3	**0.7**	-0.006	0.071	0.185	0.135	0.009	0.065	0.116
SCN-4	0.01	-0.003	**0.549**	-0.034	0.348	0.096	-0.113	-0.063
SCN-5	**0.836**	-0.012	-0.104	-0.176	-0.083	0.059	-0.039	-0.104
SCN-6	0.02	-0.247	-0.154	-0.033	0.006	**-0.513**	-0.014	-0.118
SCN-8	0.019	**0.467**	0.317	-0.151	-0.22	-0.07	0.021	-0.025
SCN-12	0.073	-0.208	-0.161	-0.172	0.053	**0.556**	-0.058	0.052
SCN-13	0.058	0.301	-0.077	-0.13	0.15	**-0.49**	0.235	0.148
SCN-16	-0.057	-0.124	0.04	0.179	-0.011	-0.227	0.054	**0.713**
SCN-17	0.057	0.092	-0.003	0.276	**0.38**	0.093	0.169	-0.024
SCN-18	0.064	0.095	0.081	-0.193	-0.054	0.08	-0.083	**0.53**
SCN-19	-0.158	0.023	-0.101	0.037	-0.162	-0.136	**-0.429**	0.02
SCN-20	0.036	0.128	0.395	**-0.418**	-0.237	0.084	0.036	-0.048
SCN-21	-0.197	-0.351	0.106	**0.463**	-0.129	0.251	0.269	0.273
SCN-22	-0.049	0.187	-0.269	0	0.081	0.293	-0.053	**0.489**
SCN-23	0.108	**0.738**	-0.148	0.215	0.019	0.01	-0.146	0.095
SCN-24	-0.014	0.086	-0.065	-0.027	-0.09	-0.045	**0.453**	0.049
SCN-25	0.019	0.167	0.039	0.247	0.039	**0.477**	0.184	-0.087
SCN-26	0.046	0.097	0.036	-0.056	**0.637**	0.063	-0.368	0.044
SCN-27	0.122	0.126	**-0.697**	-0.013	-0.038	-0.035	0.15	-0.19
SCN-28	0.042	-0.024	**0.489**	0.101	-0.108	-0.06	0.238	-0.085
SCN-30	0.038	0.106	0.014	**0.695**	-0.131	0.086	-0.041	-0.046
SCN-31	-0.097	-0.082	-0.015	-0.178	**0.714**	-0.122	0.083	-0.034
SCN-32	-0.162	-0.163	0.038	0.123	-0.062	-0.132	**0.626**	-0.229
SCN-33	-0.087	-0.052	-0.154	-0.41	0.08	0.281	**0.405**	0.19

Note: Participant-driven (i.e., noise) SCNs that were excluded from the analysis are omitted from the table (see Methods and Materials section). SCN = structural covariance network; SCP = structural covariance profile. Bolded values represent SCN loadings attributed to a specific SCP.

Table S4. Modality contributions to SCNs of SCPs.

Structural covariance profile (SCP)	Structural covariance network (SCN)	Modality contribution (%)						
		FA	**MD**	**MO**	**GMV**	**CT**	**PSA**	**Prior Weight**
SCP-1	SCN-0	0	1	0	98	0	0	1
	SCN-3	42	33	20	0	3	2	1
	SCN-5	36	16	16	0	28	4	1
SCP-2	SCN-2	52	9	10	0	27	0	1
	SCN-8	2	4	0	11	76	4	2
	SCN-23	0	0	0	78	0	16	5
SCP-3	SCN-4	64	31	0	0	3	0	1
	SCN-27	1	0	0	53	0	38	7
	SCN-28	0	75	2	0	13	0	9
SCP-4	SCN-20	3	10	18	42	6	18	3
	SCN-21	0	1	2	28	0	64	5
	SCN-30	0	27	7	0	56	0	9
SCP-5	SCN-17	7	12	20	21	16	22	3
	SCN-26	0	0	0	92	0	0	7
	SCN-31	1	23	1	0	65	0	10
SCP-6	SCN-6	21	51	16	7	3	2	1
	SCN-12	51	7	21	14	4	1	2
	SCN-13	15	11	15	41	10	5	2
	SCN-25	0	2	2	31	11	49	6
SCP-7	SCN-19	17	10	39	17	4	10	3
	SCN-24	0	20	1	38	7	28	5
	SCN-32	0	0	3	0	84	0	12
	SCN-33	0	1	9	0	0	71	18
SCP-8	SCN-16	19	8	21	24	7	18	2
	SCN-18	15	9	5	19	24	26	3
	SCN-22	5	15	16	51	8	0	4

Note: FA = fractional anisotropy, MD = mean diffusivity, MO = mode of the diffusion tensor, GMV = gray matter volume, CT = cortical thickness, PSA = pial surface area

Figure S1. **Multimodal structural covariance profiles (SCPs) and associated structural covariance networks (SCNs).** A data-reduction step was used to concatenate the multimodal SCNs into SCPs as described in Figure 1. Eight SCPs were identified with each being composed of 3-4 SCNs. The modality images displayed contribute 15% of more variance for each SCN at a Z-threshold of |2|. Warm colors (red/yellow/orange) reflect positive, and cool colors (blue/light blue) reflect relative negative, relationships of each modality with each SCN loading. Asterisks indicate modalities within an SCN that contributed a significant amount of variance but did not survive at the |2| threshold.

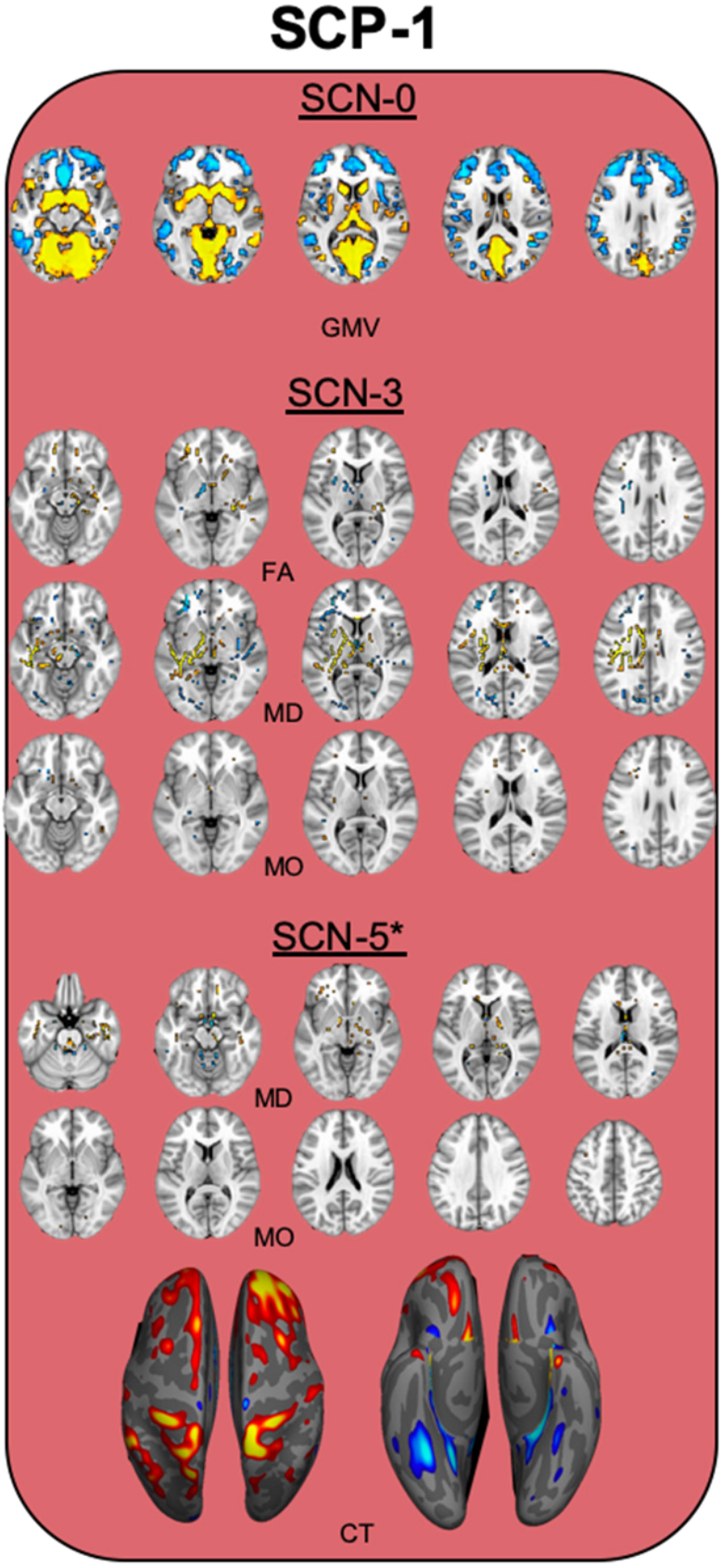
SCP-1
SCN-0
GMV
SCN-3
FA
MD
MO
SCN-5*
MD
MO
CT

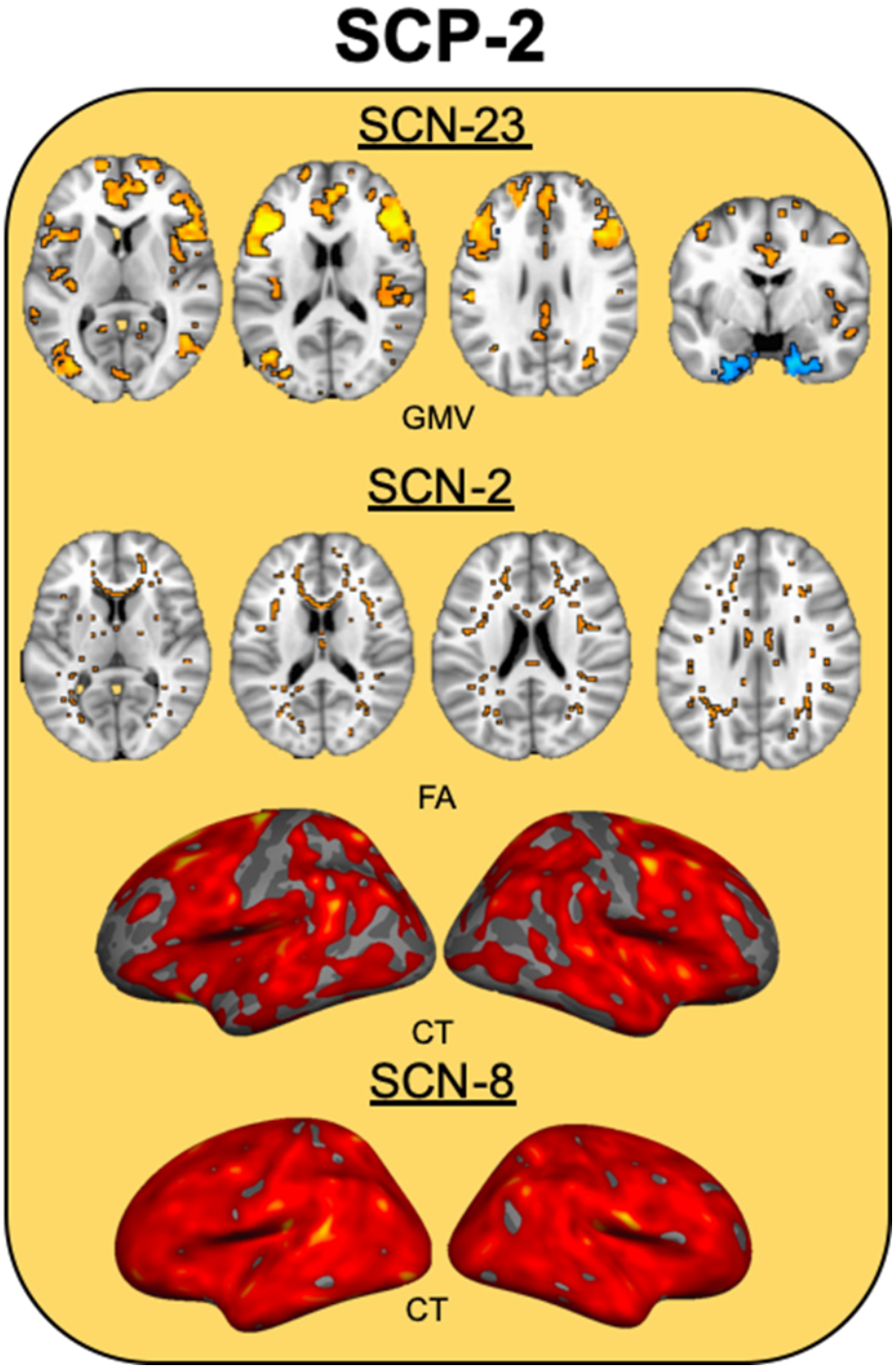
SCP-2
SCN-23
GMV
SCN-2
FA
CT
SCN-8
CT

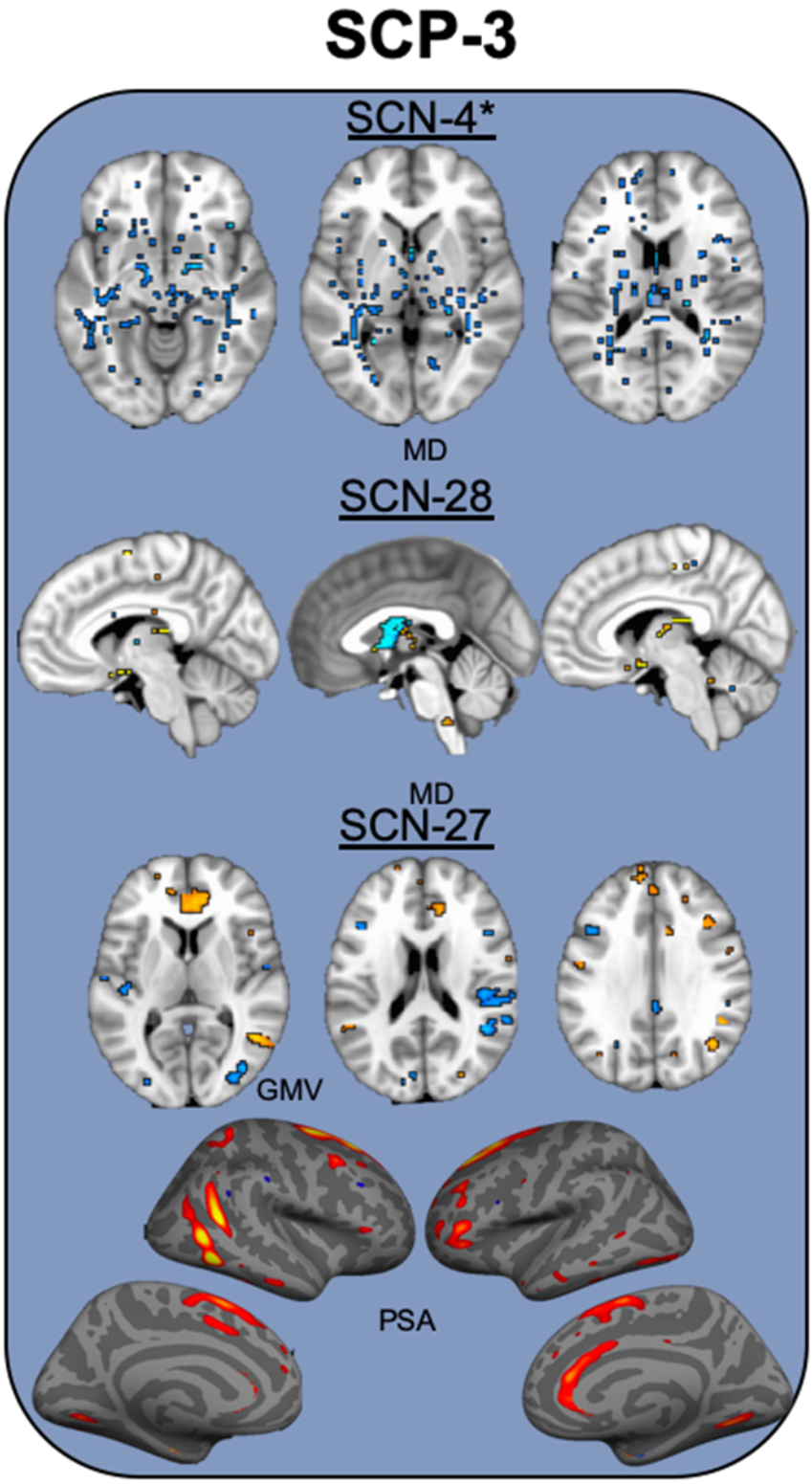
SCP-3
SCN-4*
MD
SCN-28
MD
SCN-27
GMV
PSA

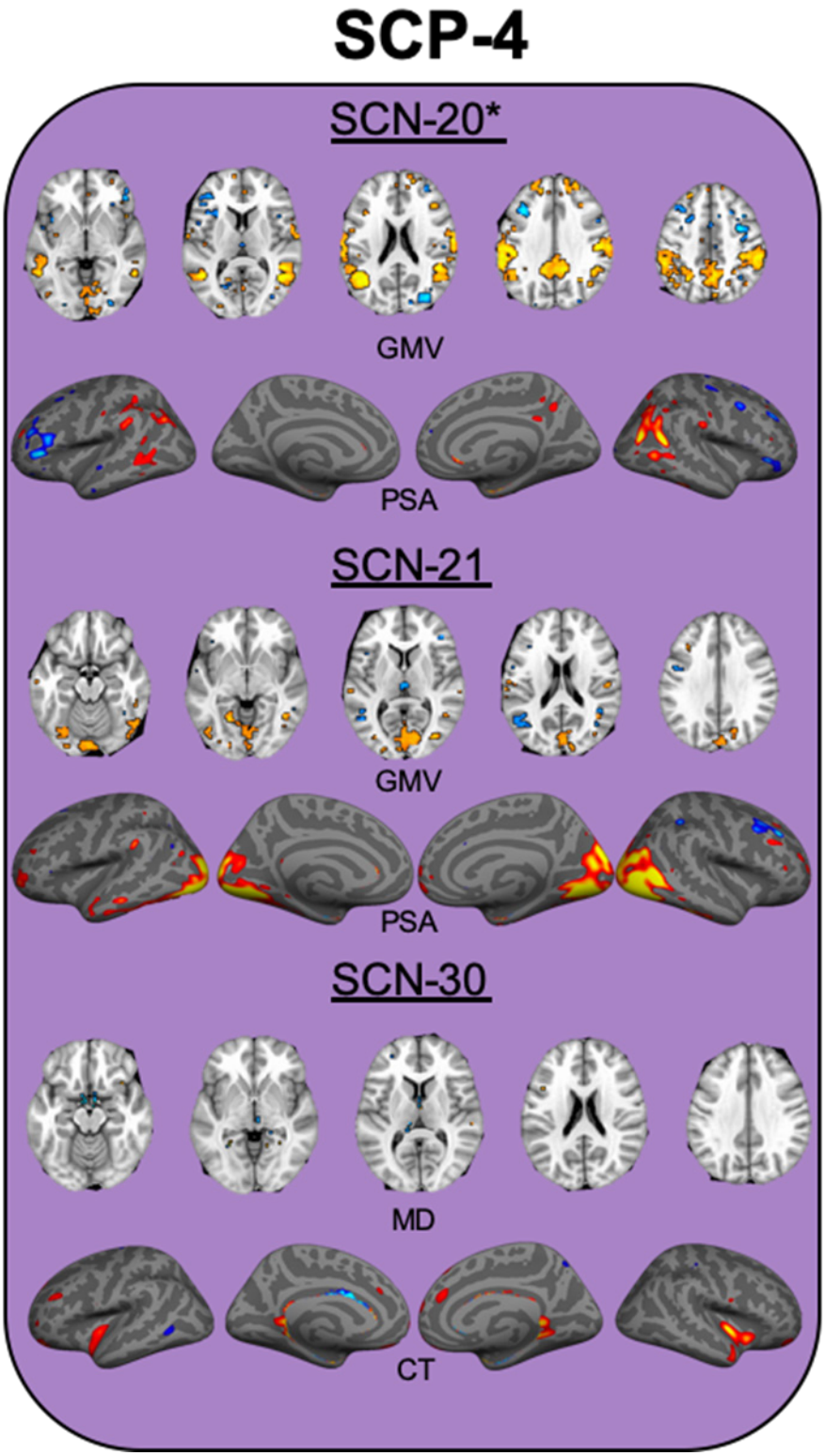
SCP-4
SCN-20*
GMV
PSA
SCN-21
GMV
PSA
SCN-30
MD
CT

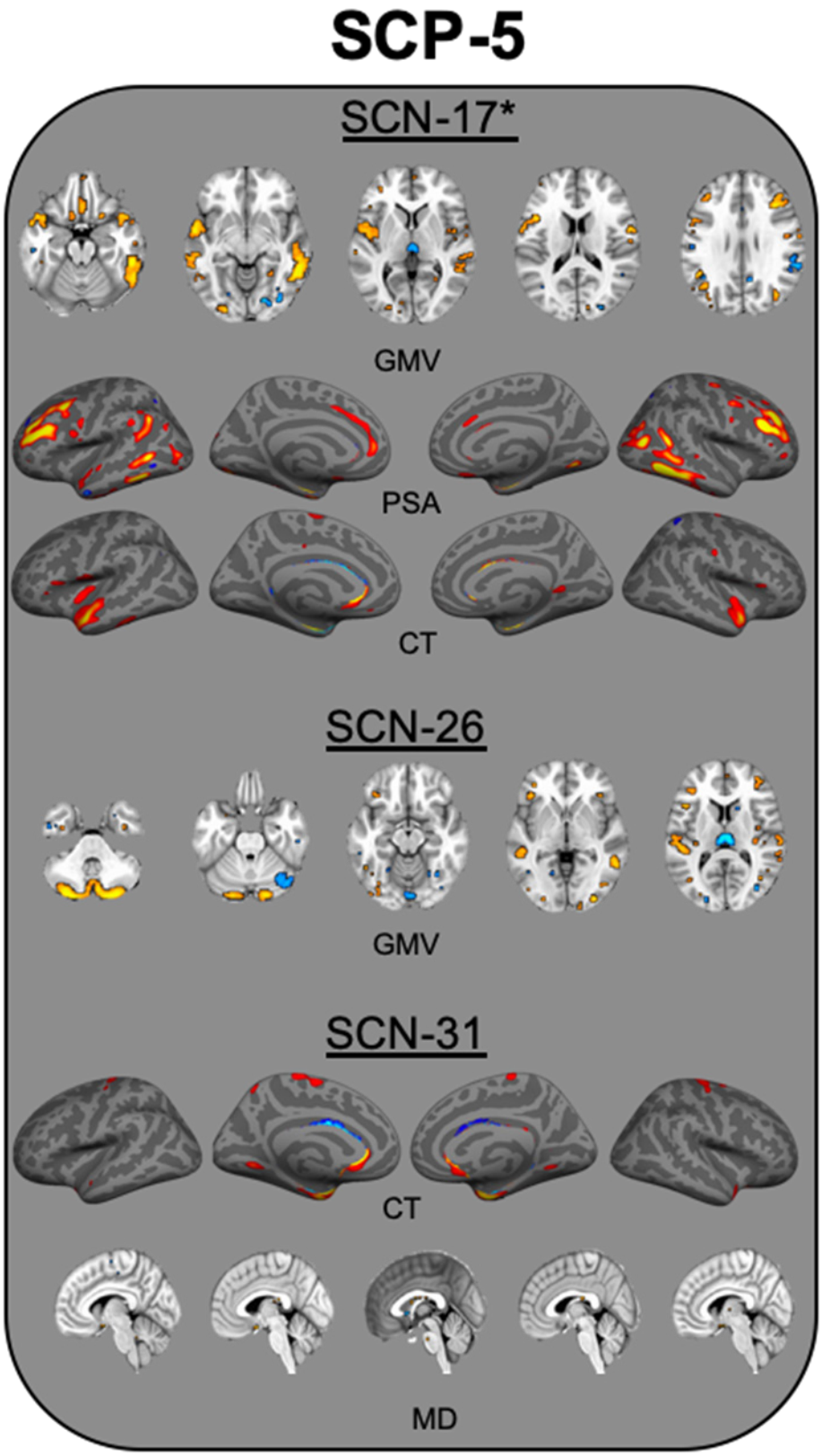
SCP-5
SCN-17*
GMV
PSA
CT
SCN-26
GMV
SCN-31
CT
MD

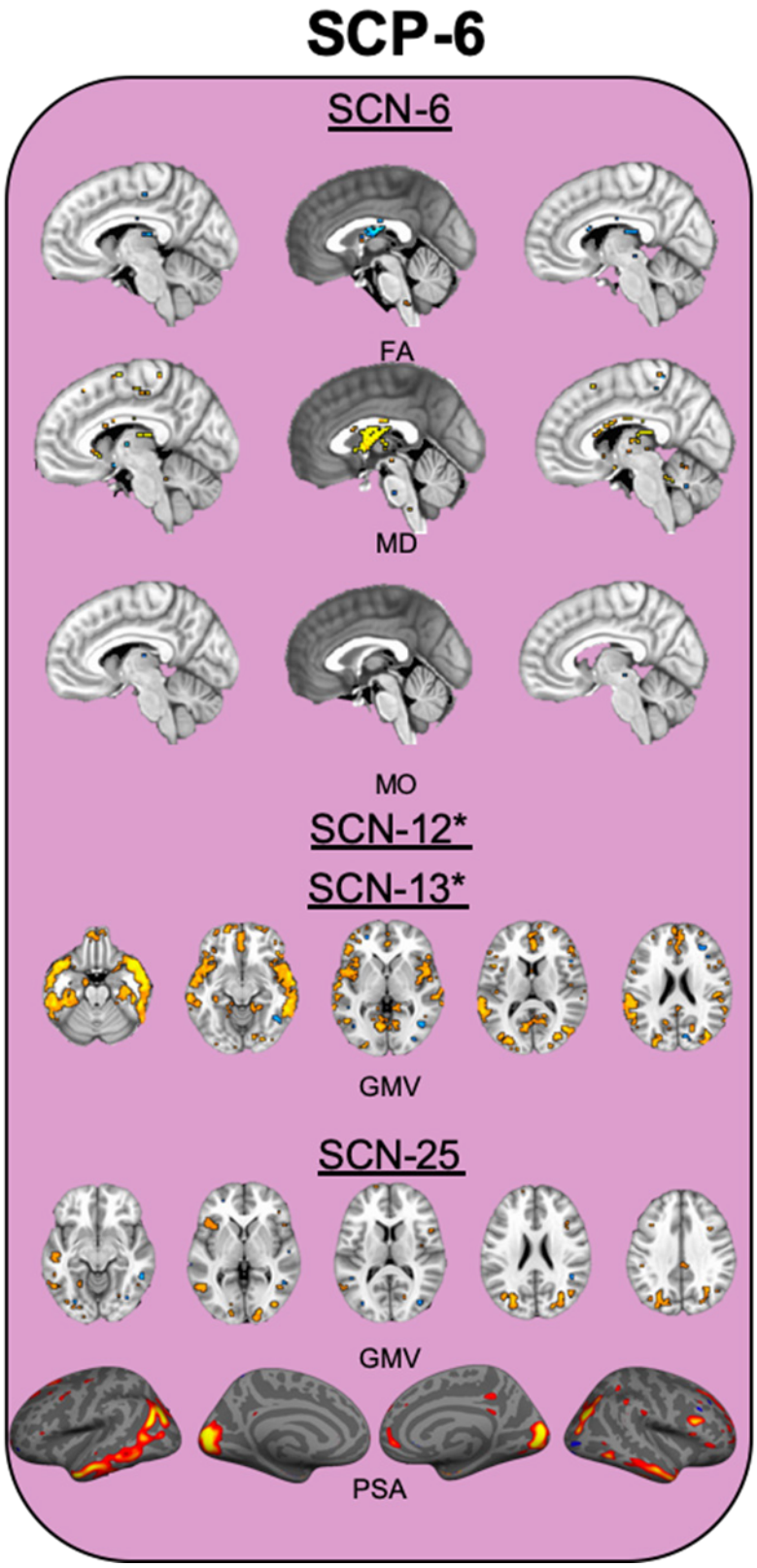
SCP-6
SCN-6
FA
MD
MO
SCN-12*
SCN-13*
GMV
SCN-25
GMV
PSA

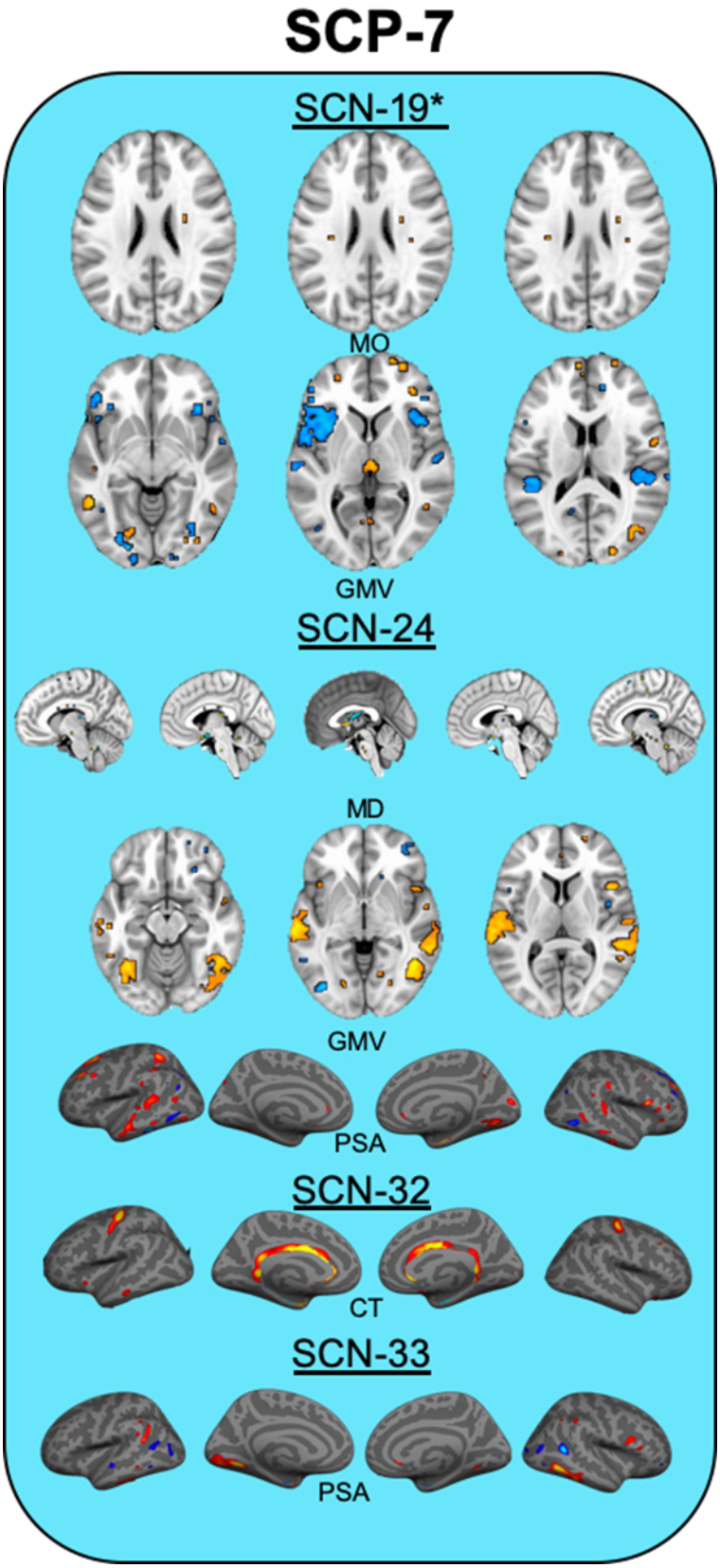
SCP-7
SCN-19*
MO
GMV
SCN-24
MD
GMV
PSA
SCN-32
CT
SCN-33
PSA

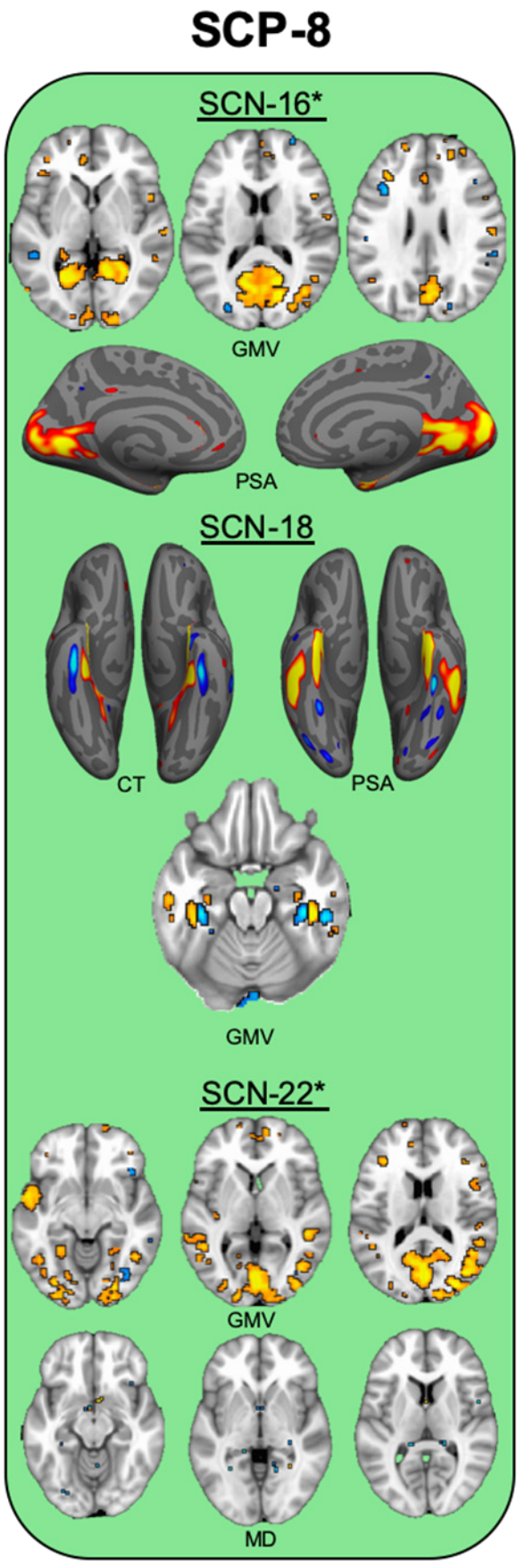
SCP-8
SCN-16*
GMV
PSA
SCN-18
CT
PSA
GMV
SCN-22*
GMV
MD

Figure S2. **Distribution of individual participant loadings for the structural covariance networks and structural covariance profiles as violin plots**. The distribution of loadings for each structural covariance network is shown in Figure S2A. The distribution of loadings for the resultant structural covariance profiles are shown in Figure S2B.

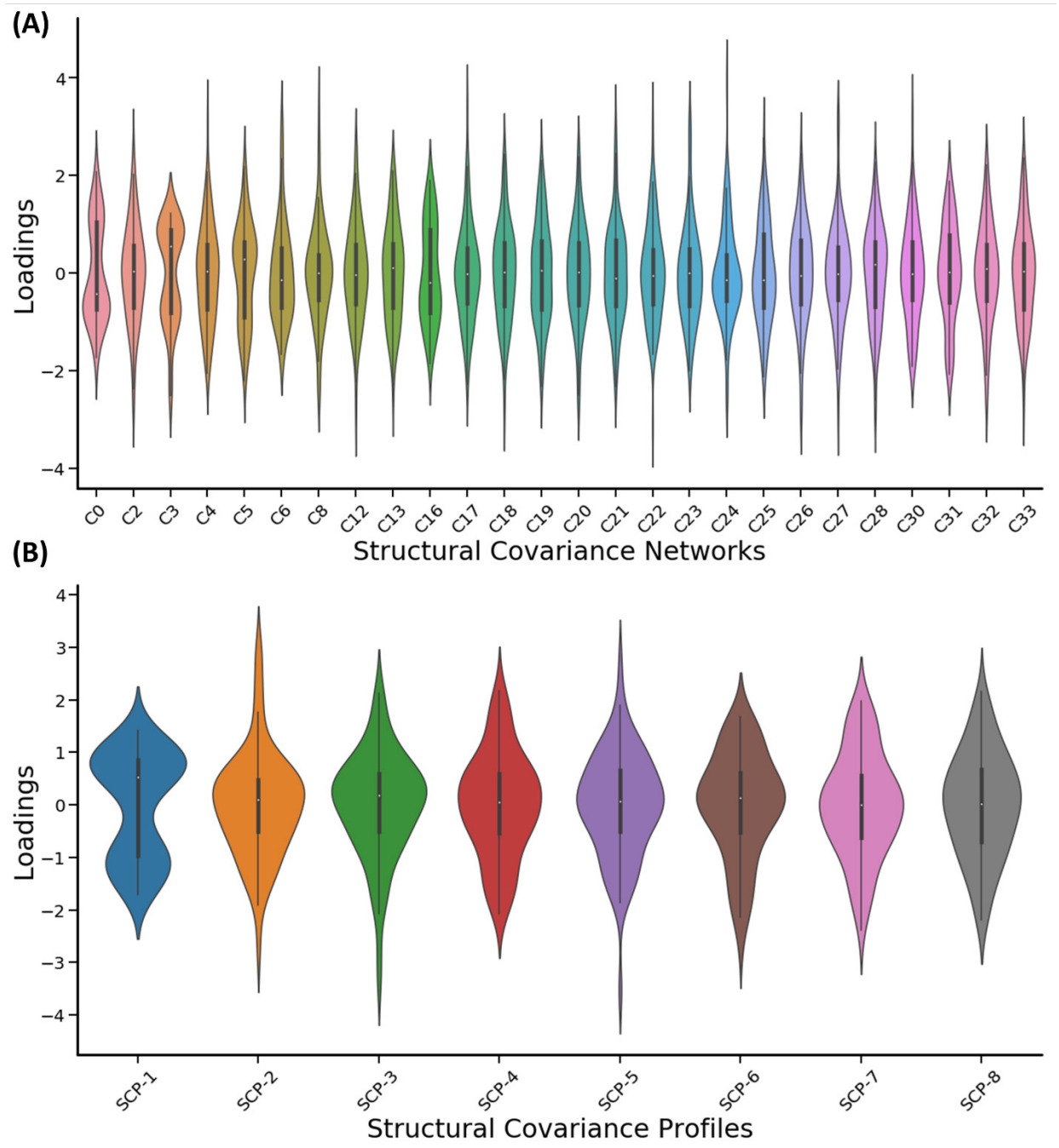

Figure S3. **Structural covariance profile three (SCP-3) is associated with acute posttraumatic stress severity.** SCP-8 varied curvilinearly with 1-month mPSS scores and the SCP reflected MD along the white matter skeleton as well as GMV/PSA of the ACC and STG. Warm colors (red/yellow/orange) reflect positive, and cool colors (blue/light blue) reflect relative negative, relationships of each modality with each SCN loading. Plots represent the standardized residuals for the SCP and mPSS scores 1 month to show the unique curvilinear relationship between the variables, accounting for covariates. Dots represent individual participant points and the solid line represents the line of best fit. Asterisks indicate other modalities contributed significant (i.e., greater than or equal to 15%) to the SCN, however no voxels survived the |2| threshold.

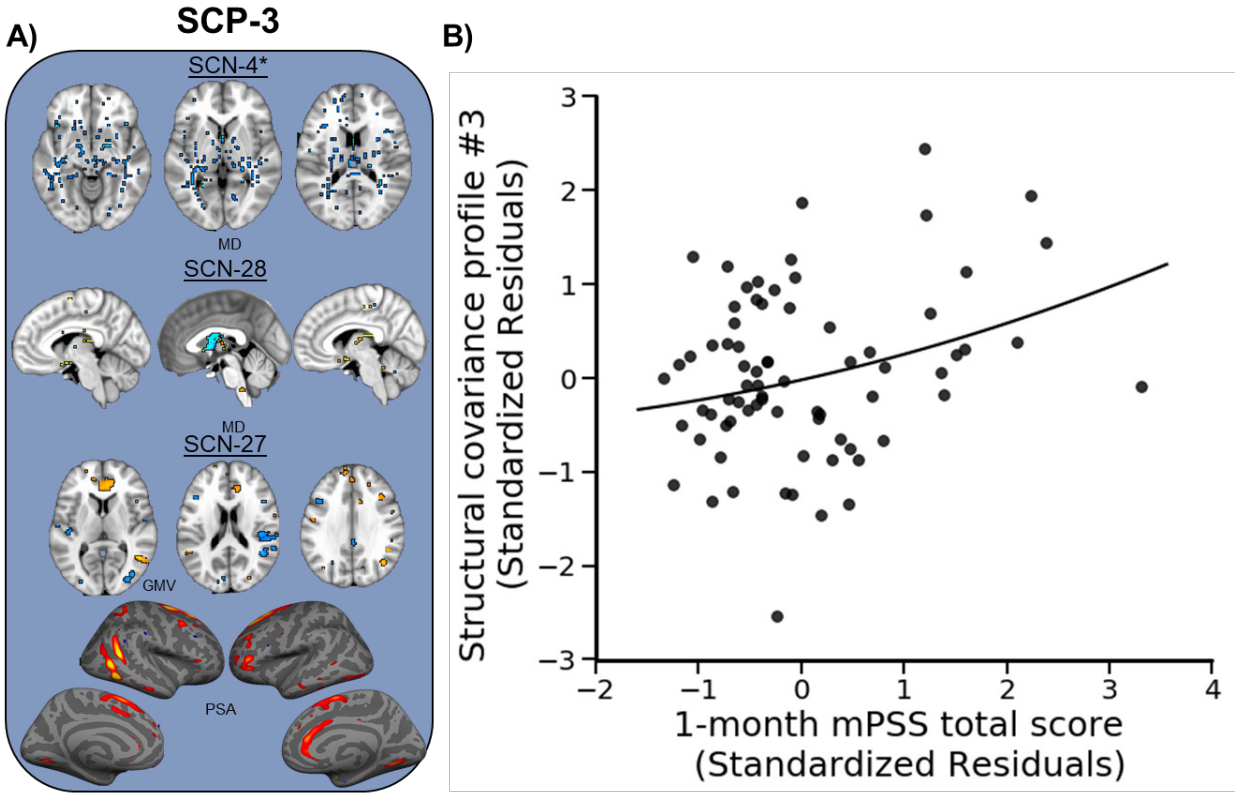

Figure S4. **Q-Q plots of significant regression models.** Residuals from the main regression analyses demonstrating the normality of the regression residuals.